

Physical and stoichiometric controls on stream respiration in a headwater stream

Jancoba Dorley¹, Joel Singley^{2,3}, Tim Covino^{4,5}, Kamini Singha⁶, Michael Gooseff^{7,8}, David Van Horn⁹, Ricardo González-Pinzón¹

Correspondence to: Ricardo González-Pinzón (gonzaric@unm.edu)

¹Civil, Construction and Environmental Engineering, University of New Mexico, Albuquerque, NM USA

²Environmental Studies Program, University of Colorado, Boulder, CO USA

³Biology, Marine Biology, and Environmental Science, Roger Williams University, Bristol, RI USA

⁴Ecosystem Science and Sustainability, Colorado State University, Fort Collins, CO USA

⁵Department of Land Resources and Environmental Sciences, Montana State University, Bozeman, MT USA

⁶Geology and Geological Engineering, Hydrologic Science and Engineering Program, Colorado School of Mines, Golden, CO USA

⁷Civil, Environmental and Architectural Engineering, University of Colorado, Boulder, CO USA

⁸Institute of Arctic and Alpine Research, University of Colorado, Boulder, CO USA

⁹Department of Biology, University of New Mexico, Albuquerque, NM USA

Abstract. Many studies in ecohydrology focusing on hydrologic transport argue that longer residence times across a stream ecosystem should consistently result in higher biological uptake of carbon, nutrients, and oxygen. This consideration does not incorporate the potential for biologically mediated reactions to be limited by stoichiometric imbalances. Based on the relevance and co-dependences between hydrologic exchange, stoichiometry, and biological uptake, and acknowledging the limited amount of field studies available to determine their net effects on the retention and export of resources, we quantified how microbial respiration is controlled by the interactions and supply of essential nutrients (C, N, P) in a headwater stream in Colorado, USA. For this, we conducted two rounds of nutrient experiments, each consisting of four sets of continuous injections of Cl⁻ as a conservative tracer, resazurin as a proxy for aerobic respiration, and one of the following nutrient treatments: a) N, b) N+C, c) N+P, and d) C+N+P. Nutrient treatments were considered as known system modifications to alter metabolism, and statistical tests helped identify the relationships between hydrologic transport and respiration metrics. We found that as discharge changed significantly between rounds and across stoichiometric treatments, a) transient storage mainly occurred in pools lateral to the main channel and was proportional to discharge, and b) microbial respiration remained similar between rounds and across stoichiometric treatments. Our results contradict the notion that hydrologic transport alone is a dominant control on biogeochemical processing and suggest that complex interactions between hydrology, resource supply, and biological community function are responsible for driving in-stream respiration.

36 **1 Introduction**

37 High biochemical processing rates in streams and rivers occur at locations and times where the dynamic
38 interconnections among hydrologic exchange, residence time, nutrient supply, and microbial biomass combine to
39 form optimum conditions for metabolic activity (i.e., the transformation of nutrients, carbon, and oxygen or another
40 electron acceptor into energy and biomass). The exchange of water between the main channel and transient storage
41 zones, where most microbes exist, is the primary mechanism supplying carbon, nutrients, and oxygen to
42 metabolically active zones (Gooseff et al. 2004; Covino et al. 2010b, 2011; Knapp et al. 2017; Gootman et al.
43 2020). The extent of water exchange controls the residence time of solutes (Drummond et al., 2012; Gomez et al.,
44 2012; Patil et al., 2013), their chemical signatures (Covino and McGlynn 2007), as well as the microbial
45 composition and their metabolic functioning (Blume et al. 2002; Navel et al. 2011; Li et al. 2020). Exchange
46 patterns are influenced by geomorphologic conditions (Kasahara and Wondzell 2003; Cardenas et al. 2004; Gooseff
47 et al. 2005; Emanuelson et al. 2022), hydrologic conditions (i.e., discharge and surrounding water table
48 configuration) (Gooseff et al. 2005; Wondzell 2006; Ward et al. 2013; Ward and Packman 2019), and biofilm
49 growth (Battin et al. 2003; Wen and Li 2018). The spatiotemporal variability in exchange processes and resource
50 availability (e.g., seasonal variations in nutrient loads) create heterogeneous hydrologic and biogeochemical
51 gradients across space and time, within which ecosystem metabolism occurs (Mulholland et al., 1985; Mulholland &
52 Hill, 1997).

53 To date, studies with a focus on hydrologic transport argue that longer residence times across a stream
54 ecosystem should consistently result in higher biological demand for carbon, nutrients, and oxygen (Valett et al.
55 1996; Gooseff et al. 2005; Wondzell 2006; Gomez et al. 2012; Zarnetske et al. 2012; Ward et al. 2013; Li et al.
56 2021), not fully incorporating the potential for biologically mediated reactions to be limited by stoichiometric
57 imbalances. Ecological stoichiometry is the notion that biota balance the consumption of nutrients with energy
58 requirements. Redfield (1934) noted that marine phytoplankton generally contained a ratio of C:N:P of 106:16:1 in
59 their biomass, and these ratios are similar to those available in their environment. This “Redfield ratio” suggests that
60 an ecosystem requires an optimal ratio of available nutrients to flourish and has been used as a guide for many other
61 environmental stoichiometry studies. In a study of streams across eight biomes, Dodds et al. (2004) noted that N
62 consumption depends in part on the C:N ratio of organic matter in streams and suggested that shifts in these state
63 ratios likely influence N retention.

64 The net effect of supply and demand of resources can be explored with the non-dimensional Damköhler
65 number, Da (Harvey et al. 2013; Pinay et al. 2015; Krause et al. 2017; Ocampo et al. 2020), which quantifies the
66 ratio of transport (i.e., supply) to biological uptake (i.e., demand) timescales along flow paths (Oldham et al. 2013;
67 Liu et al. 2022). Similar to any other non-dimensional number, Da offers simplicity and objectivity for inter-site and
68 intra-site comparisons. Da has been used to provide insight into the factors limiting the supply and demand of
69 resources (Harvey et al. 2005), as values of $Da \sim 1$ define a balance between transport and uptake time scales, which
70 theoretically result in maximal resource retention. Accordingly, where or when $Da \ll 1$, i.e., the uptake timescale is
71 much greater than the transport timescale, uptake is suboptimal, and it is referred to as reaction limited because even
72 though resources became available through hydrologic exchange, they were not fully taken up (i.e., assimilated).

73 Conversely, where or when $Da \gg 1$, i.e., the transport timescale is much greater than the uptake timescale, resources
74 become scarce or transport-limited, and biologically inactive subregions start to develop (González-Pinzón and
75 Haggerty 2013; Harvey et al. 2013; Gootman et al. 2020). While Da captures essential components of the potential
76 interactions between the supply and demand of ecologically relevant resources, it does not explicitly capture the role
77 of stoichiometric limitations on the supply (i.e., C:N:P ratios in water fluxes) and demand (C:N:P biomass
78 composition and needs) of resources (Tromboni et al. 2018). This is because Da numbers are estimated from solute-
79 specific mass balances, which inform transport and reaction timescales for one resource at a time (e.g., only N), in
80 isolation of other stoichiometrically relevant resources that can become limiting factors (e.g., C and P).

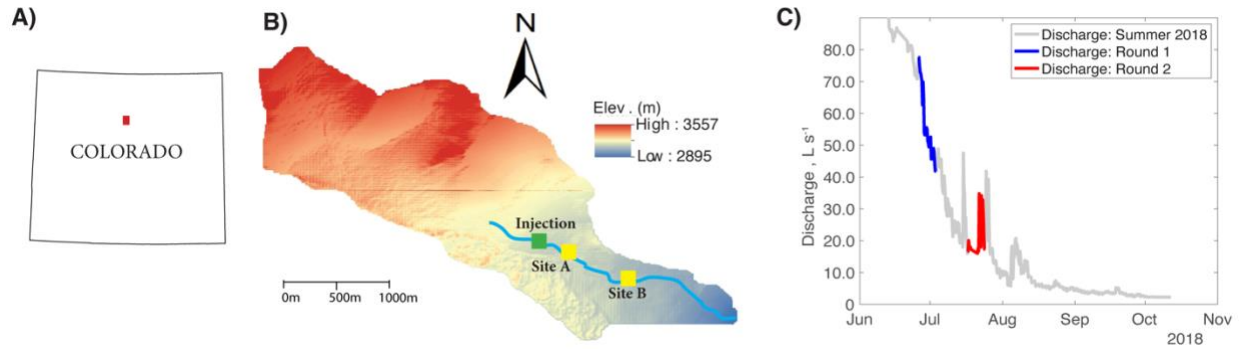
81 Based on the relevance and co-dependences between hydrologic exchange, stoichiometry, and biological
82 uptake, and the limited amount of field studies available to determine their net effects on the retention and export of
83 resources, we sought to quantify how metabolic activity is controlled by the interactions and supply of essential
84 nutrients (C, N, P). More specifically, we tested if variations in stoichiometric conditions can induce metabolic
85 limitations at which residence time alone becomes a weak predictor of stream respiration. We addressed the
86 following research question: *How is microbial respiration controlled by hydrologic exchange vs. stoichiometric*
87 *conditions (i.e., supply of C, N, and P)?* We hypothesized that aerobic respiration would be maximized when
88 nutrient supply and demand were nearly balanced for a given hydrologic condition. To test this, we conducted a
89 repeated set of stream tracer injections in Como Creek, a mountain stream in Colorado, USA, varying stream C
90 (acetate; sensu Baker et al., 1999), N (NaNO_3), and P (KH_2PO_4) concentrations to manipulate stoichiometry and
91 nutrient supply. We repeated experiments under different flow conditions to quantify the tradeoffs between supply
92 (transport and delivery of nutrients), and demand (microbial respiration). We tested for statistical relationships
93 between hydrologic transport metrics and respiration metrics using the resazurin-resorufin tracer system (González-
94 Pinzón et al., 2012; Knapp et al., 2018) and contextualized our findings within the framework of the Damköhler
95 number.

96 **2 Methods**

97 **2.1 Site Description**

98 Our research experiments were conducted in Como Creek, a forested pool and riffle stream in Colorado,
99 USA. Como Creek is a tributary to Boulder Creek, with land cover consisting of approximately 20% alpine
100 meadow-tundra and 80% conifer forest. The study reach drains a 5.4 km² catchment, with elevations ranging from
101 2895-3557 m and a mean average precipitation of 883 mm/y (Ries III et al. 2017; Emanuelson et al. 2022). Como
102 Creek has a snowmelt-driven hydrograph with stream discharges ranging from 1-98 L/s and features short-lived
103 increases in discharge during the monsoon season between July and August (Figure 1). The study reach is a multi-
104 thread channel with substrate ranging from small gravel to bedrock. Additionally, the channel has an average width-
105 to-depth ratio of 11.5, a sinuosity of 1.1, and an average longitudinal slope of 21% (Natural Resources Conservation
106 Service).

107



108
 109 **Figure 1: A) Location of Como Creek watershed in Colorado, B) detailed map of the watershed where Sites A and B are**
 110 **50 and 350 m downstream from the injection location, and C) hydrograph and timing of experimental work; each round**
 111 **of experiments consisted of four treatments featuring N, N+C, N+P, and C+N+P nutrient additions.**
 112

113 2.2 Stream tracer injection experiments

114 We conducted two rounds of experiments, each consisting of four sets of continuous injections (lasting ~ 4-
 115 7 h) of Cl⁻ as a conservative tracer, resazurin (referred to as Raz hereafter) as a proxy for aerobic respiration, and one
 116 of the following nutrient treatments: a) N, b) N+C, c) N+P, and d) C+N+P. In our study, the nutrient treatments are
 117 treated as known system modifications (control variables) to alter metabolism. Also, we use the transformation of
 118 Raz, which occurred at the same spatiotemporal scales of the nutrient additions, to calculate how changes in
 119 stoichiometric conditions and discharge affect respiration. Briefly, the reactive tracer Raz (blue in color) is
 120 irreversibly reduced to resorufin (Rru, red) under aerobic respiration, and the relationship between Raz
 121 transformation and oxygen consumption is linear (González-Pinzón et al. 2012, 2014, 2016; Knapp et al. 2018;
 122 Dallan et al. 2020).

123 Before each tracer injection, we used the Tracer Injection Planning Tool (TIPT) (González-Pinzón et al.
 124 2022) to estimate the amount of tracer mass needed to reach steady state conditions at the downstream site and to
 125 estimate the duration of the tracer breakthrough curves. From our field sampling, ambient concentrations of nitrate
 126 averaged 0.035 (±0.002) mg/L. We corroborated this value with a study by (Smith et al. 2003), who generated
 127 estimates of background total nitrogen (TN) and total phosphorous (TP) yield and concentrations throughout the
 128 stream-river network in 14 ecoregions of the conterminous US. That study found 75th % quartile TN= 0.21 (±0.05)
 129 mg/L and TP= 0.02 (±0.005), which indicates relatively low nutrient concentrations compared to agricultural
 130 streams in the US Midwest featuring ambient concentrations of up to two orders of magnitude higher. Based on
 131 estimated discharges and reach lengths, we targeted a maximum concentration of 2 mg/L for Cl, and 100 µg/L at the
 132 most downstream locations. The concentrations for nitrogen, phosphorus, and carbon were based on the expected
 133 detection limit of phosphate (i.e., 0.1 mg/L) for common ion chromatographs. From that minimum phosphate
 134 concentration expected, we scaled the masses of nitrogen and carbon using the 106C:16N:1P Redfield ratio
 135 (Redfield, 1934). Table 1 shows the masses injected and the discharges observed during the studies. Note that we
 136 allowed the stream to return to ambient concentrations for one day after each set of injections.

137
 138

139

Table 1: Tracer injection data for each round of experiments at Como Creek.

Date	Treatment	Discharge (L/s)	Start time	End time	NaCl (g)	KNO ₃ (g)	KPO ₄ (g)	Sodium Acetate (g)	Raz (g)
Round 1									
6/26/18	N	74	11:30	17:00	32653	502	-	-	150
6/28/18	N+C	61	10:08	14:10	32680	500	-	2000	150
6/30/18	N+P	53	10:00	17:00	32680	500	400	-	150
7/2/18	C+N+P	49	9:59	14:00	32680	500	400	2000	150
Round 2									
7/17/18	N	20	10:30	14:35	10000	100	-	-	30
7/19/18	N+C	17	10:00	13:59	10000	100	-	400	30
7/21/18	N+P	17	10:00	14:06	10000	100	80	-	30
7/23/18	C+N+P	25	9:30	13:35	10000	100	80	400	30

140

141

142

143

144

145

146

147

148

149

150

151

152

153

154

155

156

157

We collected 20 mL aliquots in each tracer injection 50m and 350m downstream of the injection site (labeled Sites A and B, Figure 1) to generate tracer breakthrough curves (BTCs) for Raz. All samples were filtered immediately after being collected using a 0.7 μm GF/F filter (Sigma-Aldrich) and kept on dry ice during transport until they were frozen at -4°C for laboratory analysis for Raz concentrations. All analyses took place within a week after the end of each round of injections. At the laboratory, each sample was buffered to a pH of 8.5 (1:10 buffer-to-sample) following Knapp et al. (2018). The fluorescence signals were measured with a Cary Eclipse Fluorescence Spectrophotometer (Agilent Technologies) using excitation/emission wavelengths of 602/632 nm for Raz and 571/584 nm for Rru and converted to concentrations based on an 8-point calibration curve ($R^2=0.99$).

We monitored specific conductivity (SC) and temperature using Campbell Scientific CS547A sensors connected to Campbell Scientific CR 1000 dataloggers, which recorded and stored those measurements every 10 minutes. From the grab samples, we measured chloride using a Dionex ICS-1000 Ion Chromatograph with AS23/AG23 analytical and guard columns. Cl data were augmented with background-corrected SC data to model conservative transport.

We monitored changes in stream stage every 10 minutes at the end of the study reach using pressure transducers (Campbell Scientific CS420) connected to a datalogger (Campbell Scientific CR 1000). We used established stage-discharge relationships specific for the study site, as provided by the site managers. The discharge values reported in Table 1 represent mean values observed during a given experiment.

158 2.2 Conservative transport modelling and metrics

159

160

161

162

We calibrated the conservative transport parameters of the transient storage model presented in Equations 1 and 2 using Cl^- and streamwater electrical conductivity data observed at Sites A and B. For this, we used the Matlab (The Mathworks Inc., Natick, Massachusetts) script from Knapp et al. (2018), which features a joint calibration of conservative and reactive solutes through a non-linear, least squares optimization routine.

$$163 \quad \frac{\partial c}{\partial t} = -u \frac{\partial c}{\partial x} + D \frac{\partial^2 c}{\partial x^2} - \frac{A_s}{A} \frac{\partial c_{ts}}{\partial t} + q_{in}c - \lambda_{mc}c \quad (1)$$

$$164 \quad \frac{\partial c_{ts}}{\partial t} = k(c - c_{ts}) - \lambda_{ts}c_{ts} \quad (2)$$

165

166 where c [ML^{-3}] and, c_{ts} [ML^{-3}] are the concentrations in the main channel and aggregate transient storage zone; x
 167 [L] is the distance of the study reach; t [T] is time; u [LT^{-1}] and D [L^2T^{-1}] are parameters representing advective
 168 flow velocity and dispersion coefficient, respectively; q_{in} [T^{-1}] is a volumetric flux parameter accounting for lateral
 169 inputs; k [T^{-1}] is the first-order mass transfer rate coefficient parameter between the main channel and the aggregate
 170 transient storage zone; A_s/A [-] is the capacity ratio parameter representing the relative contribution of transient
 171 storage-dominated to advection-dominated compartments in the stream, represented as areas along the reach; and
 172 λ_{mc} and λ_{ts} [T^{-1}] are processing-rate coefficients in the main channel and transient storage zones (equaling zero for
 173 a conservative tracer).

174 We completed the parameter estimation using the Differential Evolution Adaptive Metropolis (DREAM
 175 [ZS]) algorithm (Vrugt et al. 2009). We jointly fit Cl- and Raz data in a first step of 100,000 model generations. We
 176 assessed model convergence using Gelman and Rubin \hat{R} statistics (Gelman and Rubin 1992). The goodness of fit
 177 between measured and simulated BTCs was quantified through the calculation of the residual sum of squares,
 178 (nRSS) (-), normalized by the squared theoretical peak tracer concentrations of each tracer BTC of the respective
 179 tracer at the given location. The medians of the best 1,000 model simulations were used to assess the agreement
 180 between our final model fits and a subset of possible curve fits. The details on the model calibration procedure that
 181 we use in this work were presented in the supporting information of Gootman et al. (2020). Examples of observed
 182 and fitted breakthrough curves can be found in Figures S1-S3.

183 We estimated conservative transport timescales from the transport parameters to describe the transient
 184 storage timescale, $\tau_{sz} = 1/k$ [T], and the mean travel time between sites A and B, τ [T], which was computed as:

$$185 \tau = \frac{m_{1,cl}}{m_{0,cl}} \quad (3)$$

$$186 m_n = \sum_{i=1}^r \left(\frac{t_i + t_{i+1}}{2} \right)^n \left(\frac{c_i + c_{i+1}}{2} \right) (t_{i+1} - t_i) \quad (4)$$

187 where $m_{0,cl}$ and $m_{1,cl}$ are the zeroth and first-centralized temporal moments of the Cl- BTCs from each sampling
 188 site, i is a time index, r is the total number of samples available in a BTC.

189 2.3 Estimating the transformation of Raz as a proxy for microbial respiration:

190 We used the net transformation rate coefficients of Raz, λ_{Raz} [T^{-1}], as a proxy for microbial respiration, and
 191 estimated them following the work by González-Pinzón and Haggerty (2013), which derived algebraic relationships
 192 to calculate processing rate coefficients from the transient storage model presented in Equations 1 and 2:

$$193 \lambda_{Raz} = \lambda_{mcRaz} + \lambda_{tsRaz} = \frac{\ln(m_{0,Raz}^{inj}/m_{0,Raz}^{BTC})}{\tau} \left(1 + \frac{\overbrace{\ln(m_{0,Raz}^{inj}/m_{0,Raz}^{BTC})}^{\text{dispersion term, } \Phi}}{Pe} \right) \quad (5)$$

194 where $m_{0,Raz}^{inj} = M_{Raz}/Q$ is the zeroth temporal moment of Raz at the injection site [$\text{M L}^{-3} \text{T}^{-1}$], M_{Raz} is the mass of
 195 Raz added to the injectate, Q is the stream discharge [L^3T^{-1}]; $m_{0,Raz}^{BTC}$ is the dilution-corrected zeroth temporal
 196 moment of Raz estimated with BTC data from a sampling site; and $Pe = L u/D$ is the Peclet number [-], which
 197 describes the relative importance of advection and dispersion in the system.

198 Since we can only get one processing-rate coefficient from every observed BTC available from Equation
 199 (5), or from the direct calibration of the transient storage model, we expanded the work by González-Pinzón and
 200 Haggerty (2013) to incorporate the conceptual principles proposed in the Tracer Addition for Spiraling Curve
 201 Characterization (TASCC) framework (Covino et al. 2010b), where multiple rate coefficients can be estimated from
 202 an equivalent version of Equation 5.

203 Briefly, TASCC uses the dynamic range of solute concentrations sampled in BTCs to characterize uptake
 204 kinetics from ambient to saturation concentrations. In TASCC, the ratio of reactive to conservative solute
 205 concentrations for every independent sample across the tracer BTCs is compared to the ratio of the concentrations of
 206 the injection solution to determine uptake metrics. If the added solutes are non-reactive, they will transport
 207 conservatively, and the ratio of the reactive to conservative solute concentrations will remain constant. Alternatively,
 208 if the added solutes are limiting, co-limiting or reactive, they will not transport conservatively, and the ratio of the
 209 reactive to conservative solute concentrations will change over time as a function of reactivity.

210 To incorporate the TASCC framework into the algebraic equation developed by González-Pinzón and
 211 Haggerty (2013) and estimate transformation rate coefficients for Raz from each pair of conservative (i.e., $C_{cons.}$)
 212 and reactive tracer concentrations (i.e., C_{Raz}), we need to replace m_0 with $C_{Raz}/C_{cons.}$. This guarantees that the mean
 213 value of all the processing-rate coefficients is equal to the processing-rate coefficient estimated from the zeroth
 214 temporal moment analysis of model-derived simulations from Equations (1) and (2). Accordingly:

$$215 \lambda_{Raz, sample} = \frac{\ln\left[\frac{C_{Raz}}{C_{cons.}}\right]_{inj} - \ln\left[\frac{C_{Raz}}{C_{cons.}}\right]_{BTC}}{\tau} \left(1 + \frac{\overbrace{\ln\left[\frac{C_{Raz}}{C_{cons.}}\right]_{inj} - \ln\left[\frac{C_{Raz}}{C_{cons.}}\right]_{BTC}}^{dispersion\ term, \Phi}}{Pe} \right). \quad (6)$$

216 Equation 6 directly links different transport mechanisms used to explain the transport and fate of solutes
 217 (i.e., advection, dispersion, transient storage, and reactivity) with TASCC, an algorithm yielding higher information
 218 content from experimental work. We note here that alternative forms of Equation 6 can be derived for solute
 219 transport models, including additional reactions such as sorption and production. Therefore, similar new equations
 220 could be derived to provide mechanistic explanations to TASCC-related findings noticing hysteresis behavior in
 221 nutrient uptake between the rising and falling limbs of experimental BTCs (Gibson et al. 2015; Trentman et al.
 222 2015; Rodríguez-Cardona et al. 2016; Brooks et al. 2017; Day and Hall 2017). Finally, from each transformation
 223 rate coefficient $\lambda_{Raz, sample}$, we also estimated an uptake (or mass transfer) velocity of Raz, $V_{f, Raz, sample} =$
 224 $\lambda_{Raz, sample} \cdot h$, where h is the mean depth of the stream. Following Ensign and Doyle (2006), uptake velocities
 225 represent the vertical velocity of solute molecules through the water column towards the benthos and are typically
 226 used in stream ecology to normalize processing-rate coefficients by the influence from contrasting discharge
 227 magnitudes to facilitate the comparison of results from small streams and large rivers.

228 2.4 Statistical tests

229 We calculated standard deviations (std) based on repeated measures of the distribution of the transport
 230 parameters of Equations 1 and 2 to create upper and lower boundaries of the uncertainties in our measurements (i.e.,

231 mean \pm std). Because our data were not normally distributed, we used the Mann-Whitney U nonparametric statistical
232 test to determine if there were statistically significant differences between nutrient treatments across rounds (e.g., N
233 vs. N in rounds 1 and 2), following a similar procedure in Ensign and Doyle (2006). For the Mann-Whitney U test,
234 we set our significance level (α , alpha) equal to 0.05.

235 We explored the Pearson correlation coefficient (r) matrix between the transport parameters of Equations 1
236 and 2, and associated metrics, to establish direct ($r > 0.1$), inverse ($r < -0.1$), and non-existent correlations ($-0.1 < r$
237 < 0.1) (Bowley 2008). We classified the strength of the correlations as uncorrelated ($0 < r < |0.1|$), weakly correlated
238 ($|0.1| < r < |0.5|$), moderately correlated ($|0.5| < r < |0.8|$), strongly correlated ($|0.8| < r < |1.0|$), and included p-values for
239 each correlation.

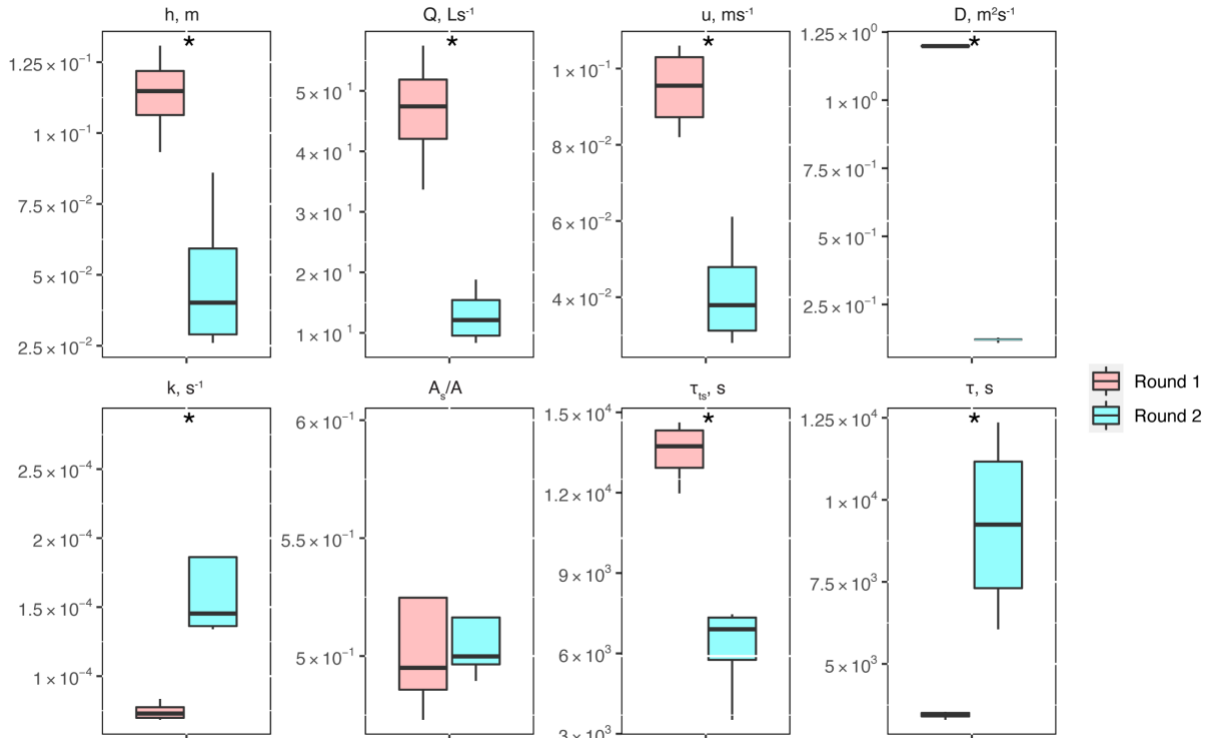
240 Lastly, we tested differences in mean values of the transport parameters of Equations 1 and 2, and
241 associated metrics, between nutrient treatments within each experimental round (e.g., N vs. N+C vs. N+P vs.
242 C+N+P in round 1) using the Student's t -test based on deviation from the group's mean value (Blair et al. 1980).

243 **3 Results and Discussion**

244 **3.1 Conservative transport and metrics of physical controls**

245 Between experimental rounds 1 and 2, stream depth (h) and discharge (Q) decreased, causing significant
246 differences in stream velocity (u), dispersion (D), mass-transfer rate coefficients (k), transient storage time scales
247 (τ_{TS}) and mean travel times (τ) (Figure 2). The only parameter that did not show significant differences was the
248 relative contribution of the main channel to storage zone areas, A_s/A .

249



250
 251 **Figure 2: Conservative transport parameters and metrics of physical controls estimated for the two experimental rounds:**
 252 **stream depth (h), stream velocity (u), dispersion (D), mass transfer rate coefficients (k), the ratio of transient storage-**
 253 **dominated to advection-dominated compartments (A_s/A), transient storage time scales (τ_{TS}) and mean travel times (τ).**
 254 **Asterisks represent statistical differences in magnitudes for rounds 1 and 2 with $p < 0.05$ (*) based on the Mann-Whitney U**
 255 **nonparametric statistical test.**

256
 257 The correlation matrix between parameters and metrics (Figure 3) shows that Q (and interrelated quantities
 258 h and u), D , and τ_{ts} were all directly correlated (from moderately to strongly). Mean travel times between sites, τ ,
 259 were directly and weakly correlated with k and the ratio A_s/A , and inversely correlated (from weakly to strongly)
 260 with the rest of the conservative transport parameters and metrics. Finally, the ratio A_s/A was generally uncorrelated
 261 or weakly correlated with other quantities. Even though the correlations of some interdependent quantities are
 262 known to be spurious, e.g., Q vs. u and λ_{RAZ} vs. V_{fRAZ} (González-Pinzón et al. 2015), we included all relevant
 263 measured and modeled quantities in Figure 3 to allow readers to explore different data pairs. For clarity, we
 264 differentiate with brackets all known spurious correlations. Note that we did not flag the correlation between A_s/A
 265 and Q (and their interrelated quantities h and u) as spurious because the ratio of areas is an indicator of the relative
 266 volume-based contribution from advection-dominated to transient storage-dominated compartments, instead of
 267 actual estimates of cross-sectional areas (Kelleher et al. 2013; González-Pinzón et al. 2013; Knapp and Kelleher
 268 2020).

269

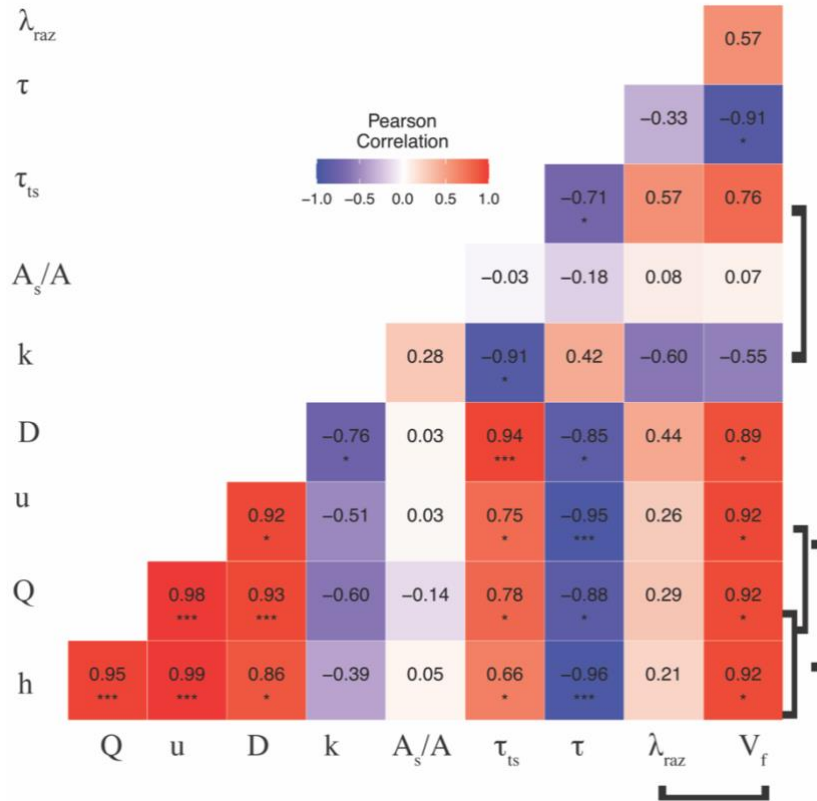


Figure 3: Pearson correlation coefficient (r) heatmap for the mean values of the transport parameters and metrics for each stoichiometric treatment during rounds 1 and 2. Brackets link known spurious correlations. Asterisks represent significant differences in magnitudes between parameters with $p < 0.05$ (*), and $p < 0.001$ (***) based on the Pearson Correlation.

One of the metrics of interest in stream reactive-transport modeling is the transient storage timescale ($\tau_{ts} = 1/k$), which quantifies the exposure that solutes have to biological communities in metabolically active transient storage zones. In our study site, τ_{ts} decreased one order of magnitude from round 1 to round 2, and were comparable to the range of values observed in other studies involving forested mountain streams (Valett et al. 1996; Hall et al. 2002). Due to the geomorphology of the stream, which is characterized by pool and riffle sequences, but steep longitudinal and valley slopes and shallow bedrock, transient storage was expected to occur mainly in the main channel (Fields and Dethier 2019; Barnhart et al. 2021; Emanuelson et al. 2022). As flow receded from round 1 to round 2, we observed the disconnection of in-stream pools contributing to transient storage, which explains the direct correlation between discharge and transient storage timescales. Another indication of the dominant contribution of in-stream pools to total transient storage is the lack of change of A_s/A with discharge. Since A is expected to vary proportional with discharge (i.e., $Q = A \cdot u$), a constant A_s/A suggests that the contribution of transient storage-dominated (i.e., A_s) compartments (i.e., A) also varied proportionally with discharge.

3.2 Raz transformation (a proxy for respiration) as a function of physical controls

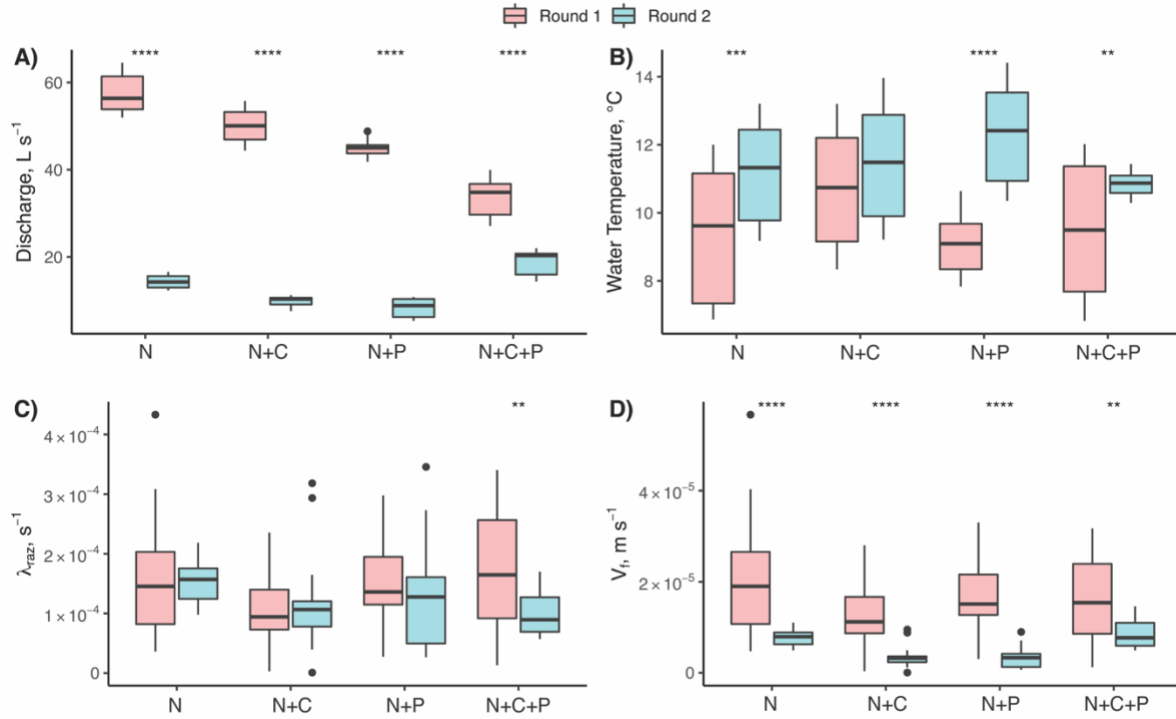
Our results indicate that the mean values of the transformation rate coefficient of Raz (λ_{Raz}) were directly and moderately correlated with the transient storage timescale (τ_{ts}), as other studies on reactive transport have

291 shown (Valett et al. 1996; Hall et al. 2002; Gomez et al. 2012; Zarnetske et al. 2012; Kiel and Bayani Cardenas
292 2014; Gootman et al. 2020). Mean λ_{Raz} values were directly and weakly correlated with discharge (Q) (also depths
293 h and velocities u) and dispersion (D), and directly and moderately correlated with τ_{ts} . Mean λ_{Raz} values were
294 inversely and weakly correlated with mean travel times (τ), and inversely and moderately correlated with mass-
295 transfer rate coefficients (k) (Figure 3). Raz uptake velocities ($V_{f_{Raz}}$) showed spurious, direct and strong
296 correlations with discharge (Q) (also h and u), strong correlations with dispersion (D) and transient storage
297 timescales (τ_{ts}), and strong indirect correlations with mean travel times (τ) and k (moderate). Finally, both λ_{Raz} and
298 $V_{f_{Raz}}$ were uncorrelated with A_s/A . Unlike studies where an increased transient storage timescale (τ_{ts}) is mainly
299 associated with slower hyporheic flows due to lower discharges (Q) (Zarnetske et al. 2007; Schmid et al. 2010), τ_{ts}
300 in our study site increased with Q because the geomorphology of the channel and the valley favored in-stream
301 transient storage in lateral pools (Jackson et al. 2012, 2013, 2015). Similar declines in transient storage with falling
302 discharge have been observed in other streams with comparable geomorphic characteristics (Covino et al. 2010a;
303 Emanuelson et al. 2022), however, the absence of concurrent declines in respiration suggest biological control by
304 some other mechanism.

305 **3.3 Raz transformation (a proxy for respiration) as a function of physical and stoichiometric controls**

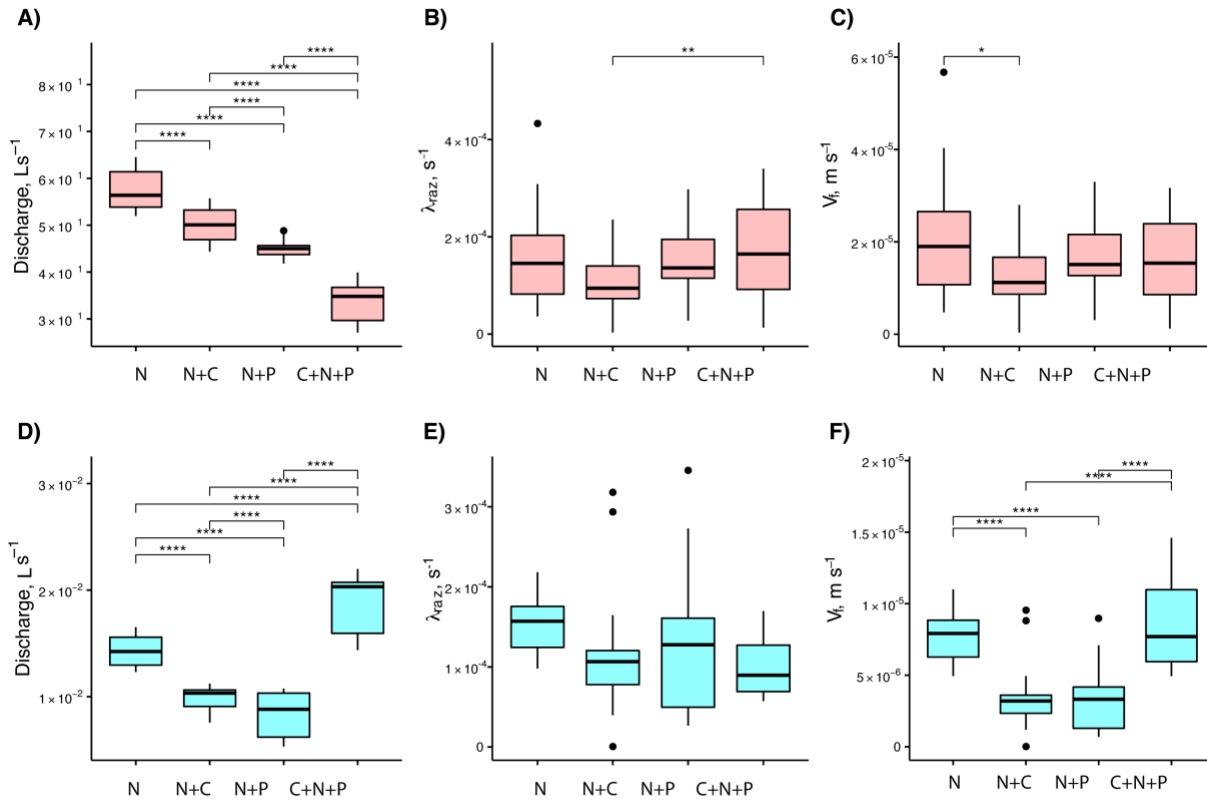
306 Our results suggest no significant changes in respiration despite significant differences in discharge (Q),
307 temperature, and nutrient treatments. Between experimental rounds, the mean values of Q (and h and u by
308 extension) and temperature (except for N+C) were statistically different for each treatment comparison (Figure 4A).
309 For λ_{Raz} , we only found statistical differences between rounds for the C+N+P treatments (Figure 4C). Due to the
310 large influence of Q on the uptake velocity of Raz ($V_{f_{Raz}}$) through stream depth (h), the statistical differences
311 between rounds seen for Q were also seen for $V_{f_{Raz}}$ (Figure 4D).

312



313
 314 **Figure 4: Comparison of A) stream discharge values recorded at the gaging station, B) stream water temperatures, C)**
 315 **transformation rate coefficients of resazurin (λ_{Raz}) resulting from Equation 6, and associated D) uptake velocities of**
 316 **resazurin ($V_{f_{Raz}} = \lambda_{Raz} h$) estimated for each experimental nutrient treatment addition during rounds 1 and 2. Due to**
 317 **the large influence of Q on the uptake velocity of Raz ($V_{f_{Raz}}$) through stream depth (h), most of the statistical differences**
 318 **between rounds seen for Q were also seen for $V_{f_{Raz}}$. Asterisks represent significant differences in magnitudes between**
 319 **rounds with $p < 0.01$ (**), and $p \sim 0$ (****) based on the Mann-Whitney U nonparametric statistical test.**
 320

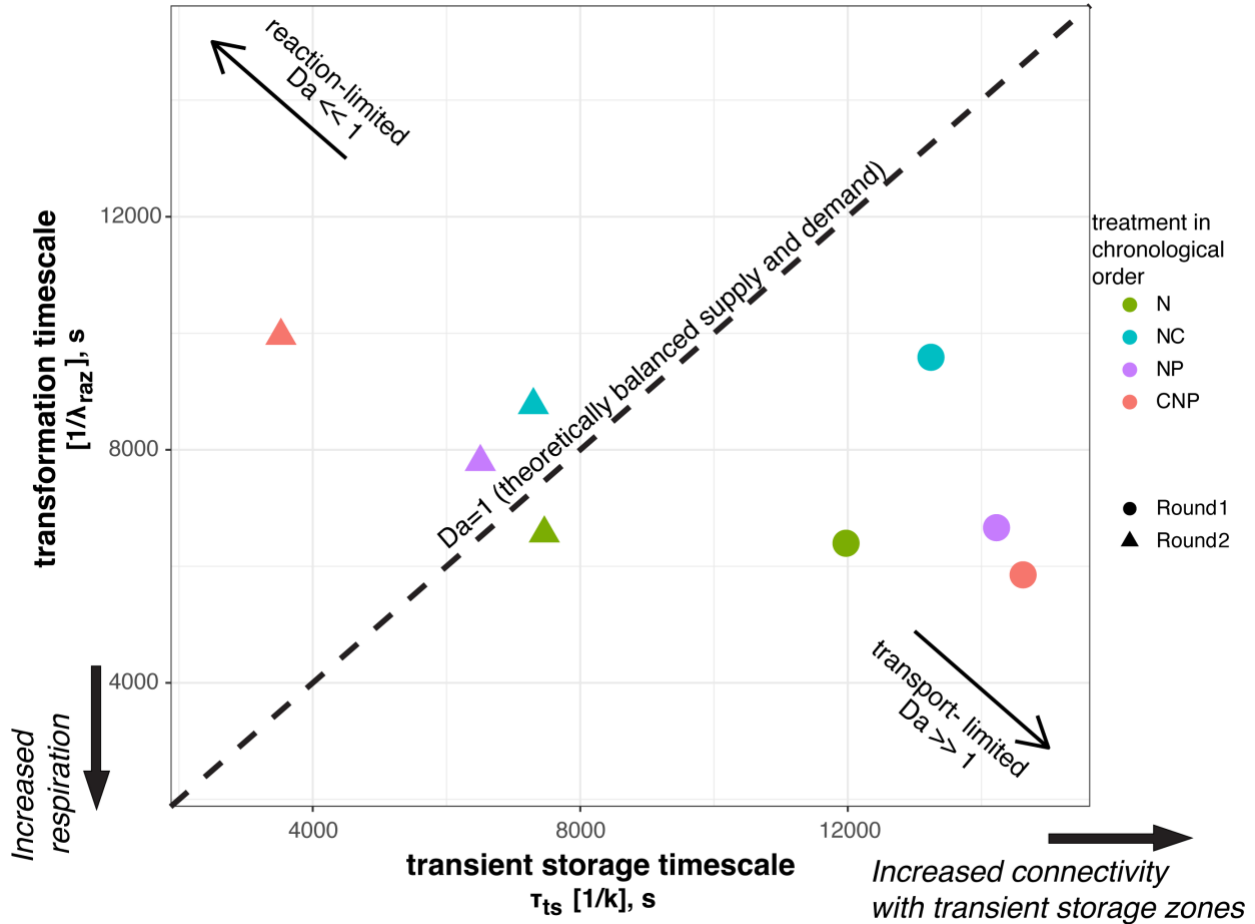
321 When looking at the data collected from each round, we found that mean Q values were statistically
 322 different across nutrient treatments (Figures 5A and 5D). For mean λ_{Raz} values, the only treatments with statistical
 323 differences were the N+C and C+N+P from round 1 (Figures 5B and 5E). Finally, $V_{f_{Raz}}$ mean values were only
 324 statistically different for the N vs N+C treatments for round 1, and for all but the N+C vs N+P and N vs C+N+P
 325 treatments for round 2 (Figures 5C and 5F).
 326



327
 328 **Figure 5: Comparison of stream discharges (A and D), transformation rate coefficients of resazurin (λ_{Raz}) (B and E), and**
 329 **uptake velocities of resazurin ($V_{f_{Raz}}$) (C and F) across treatments for round 1(top row) and 2 (bottom row). Due to the**
 330 **large influence of Q on the uptake velocity of Raz ($V_{f_{Raz}}$) through stream depth (h), most of the statistical differences**
 331 **between rounds seen for Q were also seen for $V_{f_{Raz}}$. Asterisks represent significant differences in magnitudes for**
 332 **treatments N, N+C, N+P, and C+N+P with $p < 0.05$ (*), $p < 0.01$ (**), and $p \sim 0$ (****) based on the Mann-Whitney U**
 333 **nonparametric statistical test.**

334
 335 For each of the eight nutrient injections, we related the mean transient storage timescales, τ_{ts} , which
 336 indicate exposure times between solutes and microbial communities, and the mean transformation timescales of Raz,
 337 $1/\lambda_{Raz}$, which indicate respiration (Figure 6). This Damköhler-based analysis allows us to visualize the interplay
 338 between physical, biological, and stoichiometric controls in the stream. We found that the range of variation of the
 339 mean transient storage timescales was three times greater than that of the mean transformation timescales. In round
 340 1, all the stoichiometric treatments resulted in transport-limited conditions due to the high values of τ_{ts} , i.e., the
 341 average particle of Raz that entered a metabolically active compartment underwent transformation and more Raz
 342 could have been transformed if it had been available. Thus, in round 1, respiration was high relative to the supply of
 343 solutes to the metabolically active transient storage zones. In round 2, all stoichiometric treatments, except N,
 344 resulted in reaction-limited conditions, i.e., the average particle of Raz entering a metabolically active compartment
 345 left it without undergoing transformation. Thus, in round 2, respiration was slow relative to the exposure of solutes
 346 to microbial communities.

347
 348



349
 350 **Figure 6: Mean reaction and transient storage timescales for each nutrient treatment. The Damköhler, $Da =$**
 351 **transient storage timescale/ transformation timescale, indicates reaction-limited and transport-limited conditions.**
 352

353 **3.4 How is microbial respiration controlled by hydrologic exchange vs. stoichiometric conditions (i.e., supply**
 354 **of C, N, and P)?**

355 We characterized microbial respiration with the transformation timescale of Raz, $1/\lambda_{Raz}$; the extent of
 356 hydrologic exchanges with the transient storage timescale, τ_{TS} , and the relative size of the main channel and
 357 transient storage areas, A_s/A ; and stoichiometric conditions with our controlled nutrient additions (i.e., N, N+C,
 358 N+P, and C+N+P treatments). The most salient findings indicate that a) discharge (Q) changed significantly
 359 between rounds (Figure 4a) and across stoichiometric treatments (Figure 5a, 5d), and was directly and moderately
 360 correlated with τ_{TS} and uncorrelated with A_s/A (Figure 3), suggesting that most transient storage occurred in lateral
 361 pools in the channel, which increased in quantity and extent proportionally with Q , and b) the respiration activity
 362 indicated by λ_{Raz} remained similar between rounds with significantly different Q (Figure 4b), and across controlled
 363 stoichiometric treatments also featuring different Q (Figure 5b, 5e). Thus, we observed that respiration remained
 364 largely unchanged or constant with varying physical and stoichiometric conditions.

365 Several hypotheses may explain the invariant respiration observed between experimental rounds and
 366 treatments. First, tradeoffs in metabolic rates may have occurred as the stream shifted from high to low flows. At

367 high flows during late June and early July, lateral pools in the main channel were inundated, and transient storage
368 timescales likely associated with these pools were high. Under these conditions, the observed respiration was
369 probably supported by low levels of processing in the hyporheic zone due to the prevalence of bedrock substrate and
370 relatively low respiration from benthic biomass due to scour from high flows (Francoeur and Biggs 2006; Katz et al.
371 2018). However, the combination of longer transient storage timescales and an expanded total surface area resulted
372 in moderate total respiration. In contrast, during the low flows seen in the second round of injections, surface area,
373 and transient storage timescales were decreased due to the contraction of the channel. Under these conditions,
374 biomass increased likely due to decreased scour and increased stability (Francoeur and Biggs 2006; Katz et al. 2018;
375 Cargill et al. 2021), increased water temperatures (Perkins et al. 2012), and increased processing of autochthonous
376 carbon (Wagner et al. 2017) (Figure S4). This may have supported elevated areal metabolic rates in benthic biofilms
377 (Battin et al. 2016), maintaining relatively constant respiration levels with respect to the first round of injections.

378 An alternative hypothesis to explain the consistency of the observed respiration values is that some other
379 factor constraints respiration values within a narrow range. For example, the limitation of a key nutrient or metabolic
380 resource may constrain respiration. While we designed the experiments to relieve stoichiometric constraints, it is
381 possible that the quantities of C, N, and P in the injectate we were logistically able to introduce to the stream were
382 insufficient to overcome demand. Also, the form of the resources may not have been readily available to
383 communities adapted to these locals, as stream microbial communities most efficiently process the forms and
384 diversity of dissolved organic matter found in their native habitats, and they express extracellular enzymes in ratios
385 appropriate to acquire limiting nutrients (Hill et al. 2012; Lane et al. 2012; Wilhelm et al. 2015; Logue et al. 2016).

386 In previous studies, transient storage and nutrient uptake have presented contradictory relationships, which
387 we summarize below.

388 *Inconclusive relationships:* Martí et al. (1997) did not find correlations between NH_3 uptake length and
389 A_s/A in a desert stream using data from eight tracer injections. Webster et al. (2003) did not find statistically
390 significant relationships between NH_4 uptake and A_s/A using the 11-stream LINX-I dataset that included arctic to
391 tropical streams. From thirty seven injections conducted in thirteen streams at Hubbard Brook Experimental Forest
392 (HBEF), Hall et al. (2002) found weak correlations ($R^2=0.14-0.35$) between transient storage parameters and NH_4
393 demand. Using data from seven streams in New Zealand, Niyogi et al. (2004) did not find significant correlations
394 between soluble reactive phosphorous (P-SRP), NO_3 uptake velocities, and A_s/A . Bukaveckas (2007) reported an
395 indefinite relationship between transient storage and NO_3 and P-SRP retention efficiencies from tracer injections in a
396 reference (N=13 injections), a channelized (N=14 injections), and a restored (N=17 injections) stream reach in the
397 midwestern US. Lastly, the LINX-II dataset from ^{15}N - NO_3 injections in 72 streams located in eight regions of the
398 US showed no relationship between NO_3 uptake and the fraction of median travel time due to transient storage
399 (F_{med}^{200}) (Hall et al. 2009).

400 *Weak to moderate relationships:* Thomas et al. (2003) showed that transient storage accounted for 44% to
401 49% of NO_3 retention measured by ^{15}N in a small headwater stream in North Carolina. Mulholland et al. (1997)
402 found larger PO_4 uptake rates in a stream with higher transient storage, when they compared two forested streams.
403 Ensign and Doyle (2005) found an increase in A_s/A and the uptake velocities for NH_4 and PO_4 after the addition of

404 flow baffles to two streams. Lautz and Siegel (2007) found a modest correlation ($R^2=0.44$) between NO_3 retention
405 efficiency and transient storage in the Red Canyon Creek watershed, WY.

406 *Strong relationships:* Valett et al. (1996) found a strong correlation ($R^2=0.77$) between transient storage
407 and NO_3 retention in three first-order streams in New Mexico. From nine tracer injections in two urban streams in
408 the eastern US, Ryan et al. (2007) found strong relationships between P-SRP retention and transient storage metrics
409 ($k, A_s/A$; $R^2>0.84$) when the variables were measured in different seasons. Sheibley et al. (2014) observed that the
410 retention of NO_3 in seven agricultural streams in the US was positively correlated with A_s/A and the average water
411 flux through the storage zone per unit length of stream ($q_s = kA$), and negatively correlated with the transient
412 storage timescale (τ_{ts}). However, they found no significant correlation between NH_4^+ and SRP retention and
413 transient storage metrics.

414 The studies referenced above were performed in streams with contrasting physical, chemical, and
415 biological conditions. Together, they offer a broader perspective on the inconsistent relationship between transient
416 storage metrics and metabolic processing. Those studies do not feature co-injections of C, N, and P macronutrients
417 (e.g., N+C, N+P, N+C+P), even while some tracked ambient processing rates of more than one nutrient. Therefore,
418 they generally represent solute-specific analyses, where the uptake of one nutrient at a time was analyzed and, thus,
419 did not account for stoichiometric controls on nutrient uptake (however, see Tromboni et al. (2018) for an example
420 of recent trend changes in this research area). By combining both transport and stoichiometric analyses, our study
421 offers evidence that stoichiometric controls have an ambiguous relationship to reach-scale metabolic activities, and
422 that further investigations should be conducted using greater quantities and types of resources.

423 **4 Conclusions**

424 We conducted two rounds of four stoichiometric treatments (i.e., N, C+N, N+P, and C+N+P) in a
425 headwater stream in Colorado to quantify changes to stream respiration during flow recession and answer the
426 question: *How is respiration controlled by hydrologic exchange vs. stoichiometric conditions (i.e., supply of C, N,
427 and P)?* We found that discharge changed significantly between rounds and across stoichiometric treatments, and
428 that it was directly and moderately correlated with transient storage timescales but uncorrelated with the ratio of
429 contributions from advection-dominated to transient storage-dominated compartments (i.e., A_s/A). This suggests
430 that most transient storage occurred in lateral pools within the main channel, which increased in quantity and extent
431 proportionally with discharge. We also found that respiration remained similar despite significant changes in
432 discharge and stoichiometric treatments. Our results contradict the notion that hydrologic transport alone is a
433 dominant control on biogeochemical processing, and suggest that complex interactions between hydrology, resource
434 supply, and biological community function are responsible for driving in-stream respiration.

435 **Author contribution:** RGP, TC, KS, and MG secured the funding for this research. All co-authors designed carried
436 out the experiments. JD and RGP processed Raz samples, performed solute transport simulations, statistical analyses,

437 and prepared the manuscript with input from all co-authors. DVH supported the contextualization of hydrological and
438 ecological interactions. All co-authors approved the final version of the manuscript.

439 **Competing interests:** The authors declare no competing interests.

440 **Acknowledgments**

441 The National Science Foundation provided funding support through grants NSF EAR-1642399, NSF EAR-
442 1642368, NSF EAR-1642402, NSF EAR-1642403, and NSF 1914490. We thank Karin Emanuelson, Jackie
443 Randell, Erin Jenkins, Tristan Weiss, and Melissa Pinzon for their field and laboratory assistance.

444 **Data availability:** The data used in his article can be found in the CUAHSI HydroShare repository. Gonzalez-Pinzon,
445 R. (2022). Resazurin tracer data from experiments in Colorado (2018) and Iowa (2019),
446 HydroShare, <http://www.hydroshare.org/resource/50ae3c59bebe4cb383e31408a0c10012>

447
448
449
450

451 **References**

- 452 Barnhart, T. B., J. Vukomanovic, P. Bourgeron, and N. P. Molotch. 2021. Future land cover and
 453 climate may drive decreases in snow wind-scour and transpiration, increasing streamflow
 454 at a Colorado, USA headwater catchment. *Hydrol. Process.* **35**: e14416.
 455 doi:10.1002/hyp.14416
- 456 Battin, T. J., K. Besemer, M. M. Bengtsson, A. M. Romani, and A. I. Packmann. 2016. The
 457 ecology and biogeochemistry of stream biofilms. *Nat. Rev. Microbiol.* **14**: 251–263.
 458 doi:10.1038/nrmicro.2016.15
- 459 Battin, T. J., L. A. Kaplan, J. D. Newbold, and C. M. E. Hansen. 2003. Contributions of
 460 microbial biofilms to ecosystem processes in stream mesocosms. *Nature* **426**: 439–442.
 461 doi:10.1038/nature02152
- 462 Blair, R. C., J. J. Higgins, S. Journal, and N. Winter. 1980. A Comparison of the Power of
 463 Wilcoxon ' s Rank-Sum Statistic to That of Student ' s t Statistic under Various
 464 Nonnormal Distributions Published by : American Educational Research Association and
 465 American Statistical Association Stable URL : <https://www.jstor.org/stable/1164905>
 466 REFERENCES Linked references are available on JSTOR for this article : reference #
 467 references _ tab _ contents You may need to log in to JSTOR to access the linked
 468 references . **5**: 309–335.
- 469 Blume, E., M. Bischoff, J. M. Reichert, T. Moorman, A. Konopka, and R. F. Turco. 2002.
 470 Surface and subsurface microbial biomass, community structure and metabolic activity as
 471 a function of soil depth and season. *Appl. Soil Ecol.* **20**: 171–181. doi:10.1016/S0929-
 472 1393(02)00025-2
- 473 Bowley, A. L. 2008. The Standard Deviation of the Correlation Coefficient Author (s): A . L .
 474 Bowley Source : *Journal of the American Statistical Association* , Vol . 23 , No . 161 (
 475 Mar . , 1928) , pp . 31- Published by : American Statistical Association Stable URL :
 476 <http://. J. Am. Stat. Assoc. 23: 31–34>.
- 477 Brooks, S. C., C. C. Brandt, and N. A. Griffiths. 2017. Estimating uncertainty in ambient and
 478 saturation nutrient uptake metrics from nutrient pulse releases in stream ecosystems.
 479 *Limnol. Oceanogr. Methods* **15**: 22–37. doi:10.1002/lom3.10139
- 480 Bukaveckas, P. A. 2007. Effects of Channel Restoration on Water Velocity, Transient Storage,
 481 and Nutrient Uptake in a Channelized Stream. *Environ. Sci. Technol.* **41**: 1570–1576.
 482 doi:10.1021/es061618x
- 483 Cardenas, M. B., J. L. Wilson, and V. A. Zlotnik. 2004. Impact of heterogeneity, bed forms, and
 484 stream curvature on subchannel hyporheic exchange. *Water Resour. Res.* **40**: 1–14.
 485 doi:10.1029/2004WR003008
- 486 Cargill, S. K., C. Segura, S. R. Villamizar, and D. R. Warren. 2021. The influence of lithology
 487 on stream metabolism in headwater systems. *Ecohydrology* **14**. doi:10.1002/eco.2284
- 488 Covino, T. P., B. McGlynn, and M. Baker. 2010a. Separating physical and biological nutrient
 489 retention and quantifying uptake kinetics from ambient to saturation in successive
 490 mountain stream reaches. *J. Geophys. Res. Biogeosciences* **115**: 1–17.
 491 doi:10.1029/2009JG001263
- 492 Covino, T. P., and B. L. McGlynn. 2007. Stream gains and losses across a mountain-to-valley
 493 transition: Impacts on watershed hydrology and stream water chemistry. *Water Resour.*
 494 *Res.* **43**: 1–14. doi:10.1029/2006WR005544

495 Covino, T. P., B. L. McGlynn, and R. A. Mcnamara. 2010b. Tracer Additions for Spiraling Curve
496 Characterization (TASCC): Quantifying stream nutrient uptake kinetics from ambient to
497 saturation. *Limnol. Oceanogr. Methods* 484–498. doi:10.4319/lom.2010.8.484

498 Covino, T. P., B. McGlynn, and J. Mallard. 2011. Stream-groundwater exchange and hydrologic
499 turnover at the network scale. *Water Resour. Res.* **47**: 1–11. doi:10.1029/2011WR010942

500 Dallan, E., P. Regier, A. Marion, and R. González-Pinzón. 2020. Does the Mass Balance of the
501 Reactive Tracers Resazurin and Resorufin Close at the Microbial Scale? *J. Geophys. Res.*
502 *Biogeosciences* **125**: 1–10. doi:10.1029/2019JG005435

503 Day, N. K., and R. O. Hall. 2017. Ammonium uptake kinetics and nitrification in mountain
504 streams. *Freshw. Sci.* **36**: 41–54. doi:10.1086/690600

505 Emanuelson, K., T. P. Covino, A. S. Ward, J. Dorley, and M. N. Gooseff. 2022. Conservative
506 solute transport processes and associated transient storage mechanisms: Comparing
507 streams with contrasting channel morphologies, land use and land cover. *Hydrol. Process.*
508 **36**.

509 Ensign, S. H., and M. W. Doyle. 2005. In-channel transient storage and associated nutrient
510 retention: Evidence from experimental manipulations. *Limnol. Oceanogr.* **50**: 1740–1751.
511 doi:10.4319/lo.2005.50.6.1740

512 Ensign, S. H., and M. W. Doyle. 2006. Nutrient spiraling in streams and river networks. *J.*
513 *Geophys. Res. Biogeosciences* **111**. doi:10.1029/2005jg000114

514 Fields, J. F., and D. P. Dethier. 2019. From on high: Geochemistry of alpine springs, Niwot
515 Ridge, Colorado Front Range, USA. *Hydrol. Process.* **33**: 1756–1774.
516 doi:10.1002/hyp.13436

517 Francoeur, S. N., and B. J. F. Biggs. 2006. Short-term Effects of Elevated Velocity and Sediment
518 Abrasion on Benthic Algal Communities. *Hydrobiologia* **561**: 59–69.
519 doi:10.1007/s10750-005-1604-4

520 Gelman, A., and D. B. Rubin. 1992. Inference from Iterative Simulation Using Multiple
521 Sequences. *Stat. Sci.* **7**. doi:10.1214/ss/1177011136

522 Gibson, C. A., C. M. O'Reilly, A. L. Conine, and S. M. Lipshutz. 2015. Nutrient uptake
523 dynamics across a gradient of nutrient concentrations and ratios at the landscape scale. *J.*
524 *Geophys. Res. Biogeosciences* **120**: 326–340. doi:10.1002/2014JG002747

525 Gomez, J. D., J. L. Wilson, and M. B. Cardenas. 2012. Residence time distributions in sinuosity-
526 driven hyporheic zones and their biogeochemical effects. *Water Resour. Res.* **48**: 1–17.
527 doi:10.1029/2012WR012180

528 González-Pinzón, R., J. Dorley, J. Singley, K. Singha, M. Gooseff, and T. Covino. 2022. TIPT:
529 The Tracer Injection Planning Tool. *Environ. Model. Softw.* **156**: 105504.
530 doi:10.1016/j.envsoft.2022.105504

531 González-Pinzón, R., and R. Haggerty. 2013. An efficient method to estimate processing rates in
532 streams. *Water Resour. Res.* **49**: 6096–6099. doi:10.1002/wrcr.20446

533 González-Pinzón, R., R. Haggerty, and A. Argerich. 2014. Quantifying spatial differences in
534 metabolism in headwater streams. *Freshw. Sci.* **33**: 798–811. doi:10.1086/677555

535 González-Pinzón, R., R. Haggerty, and M. Dentz. 2013. Scaling and predicting solute transport
536 processes in streams. *Water Resour. Res.* **49**: 4071–4088. doi:10.1002/wrcr.20280

537 González-Pinzón, R., R. Haggerty, and D. D. Myrold. 2012. Measuring aerobic respiration in
538 stream ecosystems using the resazurin-resorufin system. *J. Geophys. Res. Biogeosciences*
539 **117**: 1–10. doi:10.1029/2012JG001965

540 González-Pinzón, R., J. Mortensen, and D. Van Horn. 2015. Comment on “Solute-specific
541 scaling of inorganic nitrogen and phosphorus uptake in streams” by Hall et al. (2013).
542 *Biogeosciences* **12**: 5365–5369. doi:10.5194/bg-12-5365-2015

543 González-Pinzón, R., M. Peipoch, R. Haggerty, E. Martí, and J. H. Fleckenstein. 2016.
544 Nighttime and daytime respiration in a headwater stream. *Ecohydrology* **9**: 93–100.
545 doi:10.1002/eco.1615

546 Gooseff, M. N., K. E. Bencala, D. T. Scott, R. L. Runkel, and D. M. McKnight. 2005. Sensitivity
547 analysis of conservative and reactive stream transient storage models applied to field data
548 from multiple-reach experiments. *Adv. Water Resour.* **28**: 479–492.
549 doi:10.1016/j.advwatres.2004.11.012

550 Gooseff, M. N., D. M. McKnight, R. L. Runkel, and J. H. Duff. 2004. Denitrification and
551 hydrologic transient storage in a glacial meltwater stream, McMurdo Dry Valleys,
552 Antarctica. *Limnol. Oceanogr.* **49**: 1884–1895. doi:10.4319/lo.2004.49.5.1884

553 Gootman, K. S., R. G. Pinzón, J. L. A. Knapp, V. Garayburu-Caruso, and J. Cable. 2020.
554 Spatiotemporal Variability in Transport and Reactive Processes Across a First - to Fifth -
555 Order Fluvial Network Water Resources Research. 1–18. doi:10.1029/2019WR026303

556 Hall, R. J. O., E. S. Bernhardt, and G. E. Likens. 2002. Relating nutrient uptake with transient
557 storage in forested mountain streams. *Limnol. Oceanogr.* **47**: 255–265.
558 doi:10.4319/lo.2002.47.1.0255

559 Hall, R. O., J. L. Tank, D. J. Sobota, and others. 2009. Nitrate removal in stream ecosystems
560 measured by 15N addition experiments: Total uptake. *Limnol. Oceanogr.* **54**: 653–665.
561 doi:10.4319/lo.2009.54.3.0653

562 Harvey, J. W., J. K. Böhlke, M. A. Voytek, D. Scott, and C. R. Tobias. 2013. Hyporheic zone
563 denitrification: Controls on effective reaction depth and contribution to whole-stream
564 mass balance. *Water Resour. Res.* **49**: 6298–6316. doi:10.1002/wrcr.20492

565 Harvey, J. W., J. E. Saiers, and J. T. Newlin. 2005. Solute transport and storage mechanisms in
566 wetlands of the Everglades, south Florida. *Water Resour. Res.* **41**.
567 doi:10.1029/2004WR003507

568 Hill, B. H., C. M. Elonen, L. R. Seifert, A. A. May, and E. Tarquinio. 2012. Microbial enzyme
569 stoichiometry and nutrient limitation in US streams and rivers. *Ecol. Indic.* **18**: 540–551.
570 doi:10.1016/j.ecolind.2012.01.007

571 Jackson, T. R., S. V. Apte, R. Haggerty, and R. Budwig. 2015. Flow structure and mean
572 residence times of lateral cavities in open channel flows: influence of bed roughness and
573 shape. *Environ. Fluid Mech.* **15**: 1069–1100. doi:10.1007/s10652-015-9407-2

574 Jackson, T. R., R. Haggerty, S. V. Apte, A. Coleman, and K. J. Drost. 2012. Defining and
575 measuring the mean residence time of lateral surface transient storage zones in small
576 streams. *Water Resour. Res.* **48**. doi:10.1029/2012WR012096

577 Jackson, T. R., R. Haggerty, S. V. Apte, and B. L. O’Connor. 2013. A mean residence time
578 relationship for lateral cavities in gravel-bed rivers and streams: Incorporating streambed
579 roughness and cavity shape. *Water Resour. Res.* **49**: 3642–3650. doi:10.1002/wrcr.20272

580 Kasahara, T., and S. M. Wondzell. 2003. Geomorphic controls on hyporheic exchange flow in
581 mountain streams. *Water Resour. Res.* **39**: SBH 3-1-SBH 3-14.
582 doi:10.1029/2002wr001386

583 Katz, S. B., C. Segura, and D. R. Warren. 2018. The influence of channel bed disturbance on
584 benthic Chlorophyll a: A high resolution perspective. *Geomorphology* **305**: 141–153.
585 doi:10.1016/j.geomorph.2017.11.010

586 Kelleher, C., T. Wagener, B. McGlynn, A. S. Ward, M. N. Gooseff, and R. A. Payn. 2013.
587 Identifiability of transient storage model parameters along a mountain stream. *Water*
588 *Resour. Res.* **49**: 5290–5306. doi:10.1002/wrcr.20413

589 Kiel, B. A., and M. Bayani Cardenas. 2014. Lateral hyporheic exchange throughout the
590 Mississippi River network. *Nat. Geosci.* **7**: 413–417. doi:10.1038/ngeo2157

591 Knapp, J. L. A., R. González-Pinzón, J. D. Drummond, L. G. Larsen, O. A. Cirpka, and J. W.
592 Harvey. 2017. Tracer-based characterization of hyporheic exchange and benthic biolayers
593 in streams. *Water Resour. Res.* **53**: 1575–1594. doi:10.1002/2016WR019393

594 Knapp, J. L. A., R. González-Pinzón, and R. Haggerty. 2018. The Resazurin-Resorufin System:
595 Insights From a Decade of “Smart” Tracer Development for Hydrologic Applications.
596 *Water Resour. Res.* **54**: 6877–6889. doi:10.1029/2018WR023103

597 Knapp, J. L. A., and C. Kelleher. 2020. A Perspective on the Future of Transient Storage
598 Modeling: Let’s Stop Chasing Our Tails. *Water Resour. Res.* **56**: e2019WR026257.
599 doi:10.1029/2019WR026257

600 Krause, S., J. Lewandowski, N. B. Grimm, and others. 2017. Ecohydrological interfaces as hot
601 spots of ecosystem processes: ECOHYDROLOGICAL INTERFACES AS HOT SPOTS.
602 *Water Resour. Res.* **53**: 6359–6376. doi:10.1002/2016WR019516

603 Lane, C. S., D. R. Lyon, and S. E. Ziegler. 2012. Cycling of two carbon substrates of contrasting
604 lability by heterotrophic biofilms across a nutrient gradient of headwater streams. *Aquat.*
605 *Sci.* **75**: 235–250. doi:10.1007/s00027-012-0269-0

606 Lautz, L. K., and D. I. Siegel. 2007. The effect of transient storage on nitrate uptake lengths in
607 streams: an inter-site comparison. *Hydrol. Process.* **21**: 3533–3548. doi:10.1002/hyp.6569

608 Li, L., P. L. Sullivan, P. Benettin, and others. 2021. Toward catchment hydro-biogeochemical
609 theories. *Wiley Interdiscip. Rev. Water* **8**: 1–31. doi:10.1002/wat2.1495

610 Li, Z., Z. Zeng, D. Tian, and others. 2020. The stoichiometry of soil microbial biomass
611 determines metabolic quotient of nitrogen mineralization. *Environ. Res. Lett.* **15**: 034005.
612 doi:10.1088/1748-9326/ab6a26

613 Liu, S., T. Maavara, C. B. Brinkerhoff, and P. A. Raymond. 2022. Global Controls on DOC
614 Reaction Versus Export in Watersheds: A Damköhler Number Analysis. *Glob.*
615 *Biogeochem. Cycles* **36**: e2021GB007278. doi:10.1029/2021GB007278

616 Logue, J. B., C. A. Stedmon, A. M. Kellerman, N. J. Nielsen, A. F. Andersson, H. Laudon, E. S.
617 Lindström, and E. S. Kritzberg. 2016. Experimental insights into the importance of
618 aquatic bacterial community composition to the degradation of dissolved organic matter.
619 *ISME J.* **10**: 533–545. doi:10.1038/ismej.2015.131

620 Martí, E., N. B. Grimm, and S. G. Fisher. 1997. Pre- and Post-Flood Retention Efficiency of
621 Nitrogen in a Sonoran Desert Stream. *J. North Am. Benthol. Soc.* **16**: 805–819.
622 doi:10.2307/1468173

623 Mulholland, P. J., and W. R. Hill. 1997. Seasonal patterns in streamwater nutrient and dissolved
624 organic carbon concentrations: Separating catchment flow path and in-stream effects.
625 *Water Resour. Res.* **33**: 1297–1306. doi:10.1029/97wr00490

626 Natural Resources Conservation Service. Web Soil Survey. U. S. Dep. Agric.

627 Navel, S., F. Mermillod-Blondin, B. Montuelle, E. Chauvet, L. Simon, and P. Marmonier. 2011.
628 Water-Sediment Exchanges Control Microbial Processes Associated with Leaf Litter
629 Degradation in the Hyporheic Zone: A Microcosm Study. *Microb. Ecol.* **61**: 968–979.
630 doi:10.1007/s00248-010-9774-7

631 Niyogi, D. K., K. S. Simon, and C. R. Townsend. 2004. Land use and stream ecosystem
632 functioning: nutrient uptake in streams that contrast in agricultural development. *Arch.*
633 *Für Hydrobiol.* **160**: 471–486. doi:10.1127/0003-9136/2004/0160-0471

634 Ocampo, C., Oldham, C., and Sivapalan, M. 2020. Nitrate attenuation in agricultural catchments:
635 Shifting balances between transport and reaction - Ocampo - 2006 - *Water Resources*
636 *Research - Wiley Online Library.*

637 Oldham, C. E., D. E. Farrow, and S. Peiffer. 2013. A generalized Damköhler number for
638 classifying material processing in hydrological systems. *Hydrol. Earth Syst. Sci.* **17**:
639 1133–1148. doi:10.5194/hess-17-1133-2013

640 Perkins, D. M., G. Yvon-Durocher, B. O. L. Demars, J. Reiss, D. E. Pichler, N. Friberg, M.
641 Trimmer, and G. Woodward. 2012. Consistent temperature dependence of respiration
642 across ecosystems contrasting in thermal history. *Glob. Change Biol.* **18**: 1300–1311.
643 doi:10.1111/j.1365-2486.2011.02597.x

644 Pinay, G., S. Peiffer, J.-R. De Dreuzy, and others. 2015. Upscaling Nitrogen Removal Capacity
645 from Local Hotspots to Low Stream Orders' Drainage Basins. *Ecosystems* **18**: 1101–
646 1120. doi:10.1007/s10021-015-9878-5

647 Ries III, K. G., J. K. Newson, M. J. Smith, and others. 2017. StreamStats, version 4.

648 Rodríguez-Cardona, B., A. S. Wymore, and W. H. McDowell. 2016. DOC:NO₃⁻ ratios and
649 NO₃⁻ uptake in forested headwater streams. *J. Geophys. Res. Biogeosciences* **121**: 205–
650 217. doi:10.1002/2015JG003146

651 Ryan, R. J., A. I. Packman, and S. S. Kilham. 2007. Relating phosphorus uptake to changes in
652 transient storage and streambed sediment characteristics in headwater tributaries of
653 Valley Creek, an urbanizing watershed. *J. Hydrol.* **336**: 444–457.
654 doi:10.1016/j.jhydrol.2007.01.021

655 Schmid, B. H., I. Innocenti, and U. Sanfilippo. 2010. Characterizing solute transport with
656 transient storage across a range of flow rates: The evidence of repeated tracer
657 experiments in Austrian and Italian streams. *Adv. Water Resour.* **33**: 1340–1346.
658 doi:10.1016/j.advwatres.2010.06.001

659 Sheibley, R. W., J. H. Duff, and A. J. Tesoriero. 2014. Low Transient Storage and Uptake
660 Efficiencies in Seven Agricultural Streams: Implications for Nutrient Demand. *J.*
661 *Environ. Qual.* **43**: 1980–1990. doi:10.2134/jeq2014.01.0034

662 Smith, R. A., R. B. Alexander, and G. E. Schwarz. 2003. Natural background concentrations of
663 nutrients in streams and rivers of the conterminous United States. *Environ. Sci. Technol.*
664 **37**: 3039–3047. doi:10.1021/es020663b

665 Thomas, S. A., H. Maurice Valett, J. R. Webster, and P. J. Mulholland. 2003. A regression
666 approach to estimating reactive solute uptake in advective and transient storage zones of
667 stream ecosystems. *Adv. Water Resour.* **26**: 965–976. doi:10.1016/S0309-
668 1708(03)00083-6

669 Trentman, M. T., W. K. Dodds, J. S. Fencl, K. Gerber, J. Guarneri, S. M. Hitchman, Z. Peterson,
670 and J. Rüegg. 2015. Quantifying ambient nitrogen uptake and functional relationships of
671 uptake versus concentration in streams: a comparison of stable isotope, pulse, and plateau
672 approaches. *Biogeochemistry* **125**: 65–79.

673 Tromboni, F., S. A. Thomas, B. Gücker, and others. 2018. Nutrient Limitation and the
674 Stoichiometry of Nutrient Uptake in a Tropical Rain Forest Stream. *J. Geophys. Res.*
675 *Biogeosciences* **123**: 2154–2167. doi:10.1029/2018JG004538

676 Valett, H. M., J. A. Morrice, C. N. Dahm, and M. E. Campana. 1996. Parent lithology, surface-
677 groundwater exchange, and nitrate retention in headwater streams. *Limnol. Oceanogr.* **41**:
678 333–345. doi:10.4319/lo.1996.41.2.0333

679 Vrugt, J. A., C. J. F. Ter Braak, C. G. H. Diks, B. A. Robinson, J. M. Hyman, and D. Higdon.
680 2009. Accelerating Markov Chain Monte Carlo Simulation by Differential Evolution
681 with Self-Adaptive Randomized Subspace Sampling. *Int. J. Nonlinear Sci. Numer. Simul.*
682 **10**. doi:10.1515/IJNSNS.2009.10.3.273

683 Wagner, K., M. M. Bengtsson, R. H. Findlay, T. J. Battin, and A. J. Ulseth. 2017. High light
684 intensity mediates a shift from allochthonous to autochthonous carbon use in
685 phototrophic stream biofilms. *J. Geophys. Res. Biogeosciences* **122**: 1806–1820.
686 doi:10.1002/2016JG003727

687 Ward, A. S., and A. I. Packman. 2019. Advancing our predictive understanding of river corridor
688 exchange. *Wiley Interdiscip. Rev. Water* **6**: e1327. doi:10.1002/wat2.1327

689 Ward, A. S., R. A. Payn, M. N. Gooseff, B. L. McGlynn, K. E. Bencala, C. A. Kelleher, S. M.
690 Wondzell, and T. Wagener. 2013. Variations in surface water-ground water interactions
691 along a headwater mountain stream: Comparisons between transient storage and water
692 balance analyses. *Water Resour. Res.* **49**: 3359–3374. doi:10.1002/wrcr.20148

693 Webster, J. R., P. J. Mulholland, J. L. Tank, and others. 2003. Factors affecting ammonium
694 uptake in streams - an inter-biome perspective. *Freshw. Biol.* **48**: 1329–1352.
695 doi:10.1046/j.1365-2427.2003.01094.x

696 Wen, H., and L. Li. 2018. An upscaled rate law for mineral dissolution in heterogeneous media:
697 The role of time and length scales. *Geochim. Cosmochim. Acta* **235**: 1–20.
698 doi:10.1016/j.gca.2018.04.024

699 Wilhelm, L., K. Besemer, L. Fragner, H. Peter, W. Weckwerth, and T. J. Battin. 2015.
700 Altitudinal patterns of diversity and functional traits of metabolically active
701 microorganisms in stream biofilms. *ISME J.* **9**: 2454–2464. doi:10.1038/ismej.2015.56

702 Wondzell, S. M. 2006. Effect of morphology and discharge on hyporheic exchange flows in two
703 small streams in the Cascade Mountains of Oregon, USA. *Hydrol. Process.* **20**: 267–287.
704 doi:10.1002/hyp.5902

705 Zarnetske, J. P., M. N. Gooseff, T. R. Brosten, J. H. Bradford, J. P. McNamara, and W. B.
706 Bowden. 2007. Transient storage as a function of geomorphology, discharge, and
707 permafrost active layer conditions in Arctic tundra streams. *Water Resour. Res.* **43**: 7410.
708 doi:10.1029/2005WR004816

709 Zarnetske, J. P., R. Haggerty, S. M. Wondzell, V. A. Bokil, and R. González-Pinzón. 2012.
710 Coupled transport and reaction kinetics control the nitrate source-sink function of
711 hyporheic zones. *Water Resour. Res.* **48**. doi:10.1029/2012wr011894
712